Electron Parametric Instabilities of Ultraintense Short Laser Pulses Propagating in Plasmas

B. Quesnel, P. Mora, J. C. Adam, S. Guérin, A. Héron, and G. Laval

Centre de Physique Théorique (UPR 14 du CNRS), Ecole Polytechnique, 91128 Palaiseau Cedex, France

(Received 20 September 1996)

A general dispersion relation is given for electron parametric instabilities of an ultraintense circularly polarized wave propagating in a plasma. It is valid for any plasma density and wave intensity and corresponds to a generalization of the Raman, relativistic modulational, relativistic filamentation, and two-plasmons instabilities. Its numerical resolution shows different zones of instability in the wave vector space. At high intensities, the zones extend and merge, with growth rates equal to a fraction of the wave frequency. At close-to-critical density and high intensity the instability leads to strong harmonic emission. Particle-in-cell simulations confirm the analytical results. [S0031-9007(97)02675-6]

PACS numbers: 52.40.Nk, 52.35.Mw, 52.60.+h, 52.65.Rr

Recent developments of high intensity lasers have renewed the interest in electromagnetic wave propagation in the regime where the electron quiver velocity is relativistic [1]. It is well known that laser propagation in plasmas is subject to various instabilities [2], which could play an important role in advanced fusion concepts [3] and advanced accelerators [4]. In this paper, we deal with ultrashort laser pulses for which ion motion can be neglected so that only electron instabilities have to be considered. At moderate intensities, these instabilities are clearly identified as the stimulated Raman scattering (SRS), the relativistic modulational instability (RMI), the relativistic filamentation instability (RFI), and the two-plasmons decay (TPD). In the weakly relativistic regime [5–7] forward SRS and RMI have been shown to merge in a rarefied plasma [5]. In the fully relativistic regime, the one-dimensional (1D) dispersion relation has been established recently [8–10]. Its analytical and numerical solution shows a wide variety of regimes depending on the parameters a_0 and n/n_c where $a_0 = eA_0/mc^2$ is the normalized amplitude of the laser wave, n is the electron plasma density, and $n_c = m\omega_0^2/4\pi e^2$ is the critical density corresponding to the laser frequency ω_0 [9]. A study of the fully relativistic 2D case was made by Sakharov and Kirsanov in the underdense plasma case [11]. On the other hand, the TPD which normally occurs at a density $n \simeq n_c/4$ has never been studied in the relativistic regime.

In this Letter, we present the general 2D dispersion relation for circularly polarized waves in a cold plasma, valid for any laser intensity and plasma density, which includes the SRS, RMI, RFI, and TPD instabilities as limiting cases at low intensities, and the previous relativistic 1D results. The dispersion relation is obtained as an infinite Hill determinant that we solve numerically. New areas of instability are evidenced. Experimental signatures are proposed.

We use the Maxwell equations for the vector and scalar potential, the density conservation equation, and the equation of motion for the cold electron fluid [7,12],

$$\frac{\partial \mathbf{p}}{\partial t} = e\nabla\phi + \frac{e}{c}\frac{\partial \mathbf{A}}{\partial t} - \nabla(\gamma mc^2),$$

where $\mathbf{A}$ and ϕ are, respectively, the vector and the scalar potential and γ the Lorentz factor of the electron. This system admits a zero order equilibrium solution [13] in the form of a circularly polarized wave propagating in a uniform plasma ($n = n_0$) in the z direction, $\mathbf{A}_0 = \mathbf{e}_p A_0 e^{i(k_0 z - \omega_0 t)} + \text{c.c.}$, $\phi_0 = 0$, $\mathbf{p}_0 = e\mathbf{A}_0/c$ $\gamma_0 = (1 + 2e^2A_0^2/m^2c^4)^{1/2}$, with $\mathbf{e}_p = (\mathbf{e}_x \pm i\mathbf{e}_y)/\sqrt{2}$ and $\omega_0^2 = \omega_{p0}^2/\gamma_0 + k_0^2c^2$, where $\omega_{p0} = (4\pi n_0 e^2/m)^{1/2}$. With these definitions, $a_0 = 1$ corresponds to an intensity of $5 \times 10^{18}\ \mathrm{W\,cm^{-2}}$ for a 1.06 μm wavelength.

We perturb this equilibrium state with first order perturbations n_1, $\mathbf{p}_1$, $\mathbf{A}_1$, and ϕ_1. We normalize $\mathbf{A} \to e\mathbf{A}/mc^2$, $\phi \to e\phi/mc^2$, $\mathbf{p} \to \mathbf{p}/mc$, and $n \to n/n_0$, and we use the Lorentz gauge ($\nabla \cdot \mathbf{A} + c^{-1}\partial\phi/\partial t = 0$), which allows us to eliminate ϕ. This results in a linear system of differential equations on n_1, $\mathbf{p}_1$, $\mathbf{A}_1$, and ϕ_1. Using Floquet's theorem, we then expand each variable f as a sum of plane waves,

$$f = \sum_{l=-\infty}^{+\infty} f_l e^{i(\mathbf{k}+l\mathbf{k}_0)\mathbf{r} - i(\omega + l\omega_0)t} + \text{c.c.}, \qquad (1)$$

where $\mathbf{k}_0 = k_0\mathbf{e}_z$. Our system thus transforms itself to an infinite system of linear equations coupling different l's which writes

$$\omega_l^2(\mathbf{p}_l - \mathbf{A}_l) + \mathbf{k}_l(\mathbf{k}_l \cdot \mathbf{A}_l)c^2 = \frac{a_0 c}{\gamma_0}\omega_l(\mathbf{e}_p^* \cdot \mathbf{p}_{l+1} + \mathbf{e}_p \cdot \mathbf{p}_{l-1})\mathbf{k}_l, \qquad (2a)$$

 0031-9007/97/78(11)/2132(4)$10.00

$$\omega_l n_l - \frac{c}{\gamma_0}\mathbf{k}_l\cdot\mathbf{p}_l + \frac{a_0^2 c}{\gamma_0^3}\mathbf{k}_\perp\cdot\mathbf{p}_l = \frac{a_0 c}{\gamma_0}[(\mathbf{k}_\perp\cdot\mathbf{e}_p)n_{l-1} + (\mathbf{k}_\perp\cdot\mathbf{e}_p^*)n_{l+1}] - \frac{a_0^2 c}{\gamma_0^3}[(\mathbf{k}_\perp\cdot\mathbf{e}_p)\mathbf{e}_p\cdot\mathbf{p}_{l-2} + (\mathbf{k}_\perp\cdot\mathbf{e}_p^*)\mathbf{e}_p^*\cdot\mathbf{p}_{l+2}], \quad (2b)$$

$$(\omega_l^2 - \mathbf{k}_l^2 c^2)\mathbf{A}_l - \frac{\omega_{p0}^2}{\gamma_0}\mathbf{p}_l + \frac{\omega_{p0}^2 a_0^2}{\gamma_0^3}\mathbf{p}_{l\perp} = \frac{\omega_{p0}^2 a_0}{\gamma_0}(n_{l+1}\mathbf{e}_p^* + n_{l-1}\mathbf{e}_p) - \frac{\omega_{p0}^2 a_0^2}{\gamma_0^3}[(\mathbf{p}_{l+2}\cdot\mathbf{e}_p^*)\mathbf{e}_p^* + (\mathbf{p}_{l-2}\cdot\mathbf{e}_p)\mathbf{e}_p], \quad (2c)$$

with $\omega_l = \omega + l\omega_0$, $\mathbf{k}_l = \mathbf{k}_\perp + (k_z + lk_0)\mathbf{e}_z$. A similar set of equations was obtained in Ref. [11].

In the following, for any vector $\mathbf{u}$ we write $\mathbf{u} = u^+\mathbf{e}_p + u^-\mathbf{e}_p^* + u^z\mathbf{e}_z$. As the problem is globally invariant under rotation along the z axis, we choose $\mathbf{k}_\perp = k_\perp\mathbf{e}_x = (k_\perp/\sqrt{2})(\mathbf{e}_p + \mathbf{e}_p^*)$.

If we first restrict ourselves to the 1D case ($k_\perp = 0$), the variables $X_l = (A_{l+1}^+, p_{l+1}^+, A_l^z, n_l, p_l^z, A_{l-1}^-, p_{l-1}^-)$ are coupled together but decoupled from the other ones. Moreover, the equations for the variables X_{l+1} are exactly similar to the ones for the set X_l, provided one replaces ω by $\omega - \omega_0$ and k_z by $k_z - k_0$. We can therefore specialize to the set X_0, in which we recognize the familiar Stokes and anti-Stokes components of the vector potential and the perturbation of electronic density and scalar potential, together with their accompanying effect on the electrons momentum. The system may then be solved analytically, and after some algebra, one recovers the 1D relativistic fully dispersion relation [8–10].

We now focus our attention on the general three-dimensional case, e.g., $k_\perp \neq 0$. All sets of variables are now coupled through a five term recurrence relation that we write in matricial form,

$$AX_{l-2} + B_l X_{l-1} + C_l X_l + D_l X_{l+1} + EX_{l+2} = 0, \quad (3)$$

where A, B_l, C_l, D_l, and E are 7×7 matrices, with A, B_l, D_l, and $E = 0$ if $k_\perp = 0$. The coefficients of the 5 matrices are functions of the parameters a_0, n_0, ω, k_z, and $k_\perp$. They can be deduced from (2).

To numerically solve (3), we truncate the recurrence, neglecting all terms with $l > L$ or $l < -L$. (The numerical values of the result are independent of L as soon as L is large enough. $L = 7$ is sufficient for the ranges of k_z and $k_\perp$ considered in this paper. The numerical absolute error [14] was found to be smaller than 10^{-6}.) We thus have to solve

$$MX = 0, \quad (4)$$

where X is a $7\times(2L+1)$ vector and M a $[7\times(2L+1)]^2$ matrix,

$$X = \begin{pmatrix} X_{-L} \\ \vdots \\ X_l \\ \vdots \\ X_L \end{pmatrix} \text{ and } M = \begin{pmatrix} C_{-L} & D_{-L} & E & & (0) \\ & \ddots & & & \\ A & B_l & C_l & D_l & E \\ & & & \ddots & \\ (0) & & A & B_L & C_L \end{pmatrix}.$$

We then first multiply each line in M that comes from (2b) by ω_l, we add (2c) to (2a), and we collect terms with the same power of ω, so that (4) now writes $-\mathbb{1}(\omega X)\omega + N(\omega X) + PX = 0$, where N and P are independent of ω. We end up with an eigenvalue problem,

$$\begin{pmatrix} 0 & \mathbb{1} \\ P & N \end{pmatrix}\begin{pmatrix} X \\ \omega X \end{pmatrix} = \omega\begin{pmatrix} X \\ \omega X \end{pmatrix}. \quad (5)$$

Therefore, for given physical parameters a_0 and n_0, the system will be parametrically unstable to perturbations at wave vector $\mathbf{k}$ if the matrix on the left-hand side of (5) has complex eigenvalues. Because of the symmetry between the terms l and $l+1$ already pointed out, there will be $2L+1$ such eigenvalues, with real parts spaced by ω_0 (in the limit L large). By continuity with the 1D case, we select the one whose real part lies between 0 and 1. The corresponding eigenvector gives us the relative amplitude of the different modes l.

We first verified that we recover the known results in the case of underdense ($n_0 \ll 1$) plasmas and of not too high ($a_0 \lesssim 0.1$) intensities of the laser [5] with slight modifications due to the circular polarization. At low density and higher intensities, we found new zones of instability in the $(k_z, k_\perp)$ plane. Their shape is semicircular and well described by the equation $(k_z - Nk_0)^2 + k_\perp^2 = N^2(\omega_0/c)^2$, $N \geq 2$, as can be seen in Fig. 1(a), for which $a_0 = 1.46$ and $n_0/n_c = 5\times 10^{-3}$. Each lobe corresponds to a resonance with a different harmonic of the vector potential through a three-wave process, as pointed out by Sakharov and Kirsanov [11]. This is seen in Fig. 2 (curve A), which shows the relative intensities of the different components of the vector potential [see Eq. (1)] in the Coulomb gauge for a mode $\mathbf{k}$ taken in the third lobe $[(k_z c/\omega_0, k_\perp c/\omega_0) = (5, 2.2)]$. The Coulomb gauge $[\mathbf{A}_C = \mathbf{A}_L - (\mathbf{k}\cdot\mathbf{A}_L)\mathbf{k}/|\mathbf{k}|^2]$ is convenient for the separation of the electrostatic (ES) and electromagnetic (EM) parts of the products of the instability. Here $\mathbf{A}_C$ and $\mathbf{A}_L$ correspond to the vector potential in the Coulomb and Lorentz gauge, respectively. We also plot in Fig. 3 the exact maximum growth rate in the first and second lobes as a function of the scattering angle of the radiated electromagnetic wave, and we find a good agreement with the estimated ones given in Ref. [11].

Our analytical calculation also describes the TPD, as can be seen from (2) taken in the nonrelativistic limit: for $\omega_0 = 2\omega_{p0}$, we only need to consider the resonant $l = 0$ and $l = -1$ terms, and a straightforward calculation gives the well-known formula for the growth rate [2]. In the relativistic regime ($a_0 \gtrsim 0.5$), the TPD unstable region in the $(k_z, k_\perp)$ plane breaks into different zones reminiscent of the half circle zones described earlier, while the domain

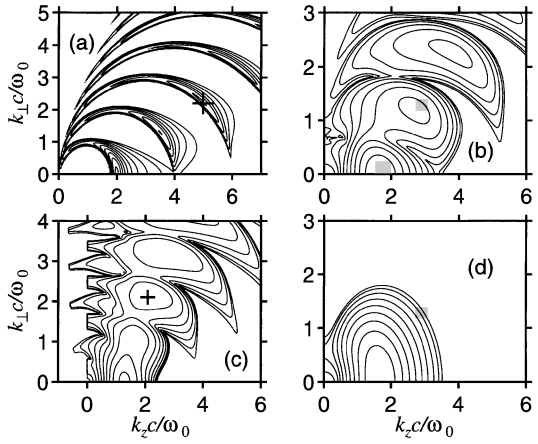

FIG. 1. Contour plot of the growth rate as a function of the wave number $(k_z, k_\perp)$. The parameters are (a) $a_0 = 1.46$ and $n_0/n_c = 5 \times 10^{-3}$, (b) $a_0 = \sqrt{3/2}$ and $n_0/n_c = 0.5$, (c) $a_0 = \sqrt{3/2}$ and $n_0/n_c = 1.5$. (d) shows the growth rate for the same parameters as (b) but calculated from the naïve 2D extension of Refs. [8–10]. There are 10 contours on each plot, the minimum and maximum being, respectively, (a) 0.01, 0.1; (b) and (d) 0.04, 0.4; (c) 0.035, 0.35. The crosses correspond to the points used to draw Fig. 2. The grey areas are the domains of wave vector used to draw Fig. 4.

of densities where TPD occurs extends widely around $n_0 = \gamma_0 n_c/4$. A typical result is shown in Fig. 1(b), which corresponds to $a_0 = \sqrt{3/2}$ and $n_0/n_c = 0.5$ (i.e., $n_0/\gamma_0 n_c = 0.25$). We emphasize here that the naïve 2D extension of the 1D fully relativistic dispersion relation [8–10] (in which one simply replaces $k_z \mathbf{e}_z$ by $\mathbf{k}$) does not predict any of the successive TPD lobes, as can be clearly seen in Fig. 1(d) which shows the growth rate as predicted by this naïve extension for the same parameters as Fig. 1(b). Correlatively, the ES character of the instability evolves towards a mixed EM/ES character. Although they decrease with $|\mathbf{k}|$, the growth rates on the successive lobes remain a significant fraction of the pump wave frequency, even for large $|\mathbf{k}|$ [$\gamma = 0.3\omega_0$ for $(k_z c/\omega_0, k_\perp c/\omega_0) = (2.7, 1.2)$ in Fig. 1(b)].

In the induced transparency regime [15] ($n_c \le n_0 < \gamma_0 n_c$), the different zones of instability already described tend to merge and new lobes appear that extend in the $k_z < 0$ region [see Fig. 1(c) for which $a_0 = \sqrt{3/2}$ and $n_0/n_c = 1.5$]. The successive lobes in the wave-vector plane are no more associated with a single harmonic as in the very underdense case [11], but a wide range of harmonics are simultaneously excited, as shown in Fig. 2, curve *B*, which corresponds to $(k_z c/\omega_0, k_\perp c/\omega_0) = (2.08, 2.1)$. Note that the real part of the frequency associated with these harmonics is $\Re(\omega_l) = |\Re(\omega) + l\omega_0|$, with $\Re(\omega) = 0.4\omega_0$ for the parameters of Fig. 2, curve *B*. As in Fig. 1(b), we have verified that the products of the instability have a mixed feature (ES/EM). In all regimes, the growth rate is maximum on axis, but takes significant values for high $k_\perp$.

This harmonic generation could provide an experimental signature of the instability. For the parameters of Figs. 1(c) and 2, curve *B*, the dominant electromagnetic mode corresponds to $l = -3$ and has a real frequency $\Re(\omega_l) = 2.6\omega_0$. It represents a backscattered wave propagating at an angle of $\theta = 105°$ with respect to $\mathbf{k}_0$ in the plasma, which will be able to escape the interaction region and be detected. If we also consider the other components with high enough frequency to escape from the plasma, one should observe as well side scattered harmonics with frequencies $1.4\omega_0$, $1.6\omega_0$, $2.4\omega_0$, and $3.4\omega_0$ corresponding, respectively, to $l = 1$, -2, 2, and 3 and $\theta = 39°, 117°, 34°$, and 30°. It must be stressed here that this instability produces backscattered light even for $0.25 < n_0/\gamma_0 n_c < 1$, an effect which has no equivalent in terms of classical theory of Raman backscattering.

The RFI (for $k_z = 0$), which is hardly visible in Fig. 1(a), gets a significant growth rate at high density in the relativistic regime [Figs. 1(b) and 1(c)], with large values of $k_\perp$. For the parameters of Fig. 1(c) the growth of this filamentation instability reaches $0.14\omega_0$ for $k_\perp c/\omega_0 = 1.5$. The growth rate curve as a function of $k_\perp$ shows a succession of narrow peaks around $k_\perp c/\omega_0 = 1.5, 2, 2.5, 2.9$, etc., with a slow decrease.

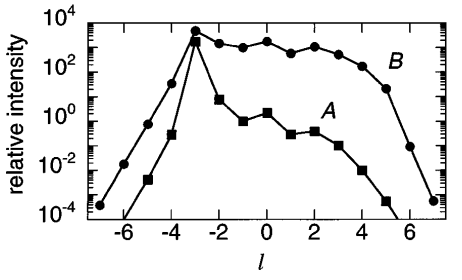

FIG. 2. Relative intensities of the different components of the vector potential in the Coulomb gauge. All components are normalized to the $l = -1$ one which corresponds to the Stokes wave. Both curves are taken on the third lobe of the instable region, respectively, curve *A*: $a_0 = 1.46$, $n_0/n_c = 5 \times 10^{-3}$, and $(k_z c/\omega_0, k_\perp c/\omega_0) = (5, 2.2)$, curve *B*: $a_0 = \sqrt{3/2}, n_0/n_c = 1.5$, and $(k_z c/\omega_0, k_\perp c/\omega_0) = (2.08, 2.1)$. Data on curve *B* have been multiplied by 10^3 to make the reading more convenient. Full lines are guides for the eyes. The real parts of the frequency are, respectively, $0.045\omega_0$ for *A* and $0.4\omega_0$ for *B*.

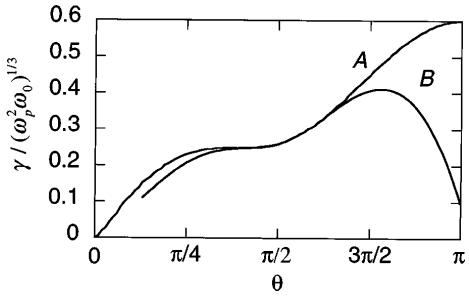

FIG. 3. Maximum growth rate as a function the scattering angle for the case of Fig. 1(a), in the first (curve *A*) and second (curve *B*) lobes. The corresponding parameter v_E/c of Ref. [11] is 0.9.

We were able to confirm these results using a $2D\frac{1}{2}$ particle in cell (PIC) code with periodic boundary conditions. The system was chosen to be $128c/\omega_0 \times 128c/\omega_0$, with $dx = dz \sim 0.17c/\omega_0$, allowing a sufficient number of modes in **k** space and the correct handling of modes with large wave numbers up to $k \sim 4\omega_0/c$. The simulation used ten particles per cell and about 6×10^6 particles in the system. The initial temperature was 2 keV. We set at $t = 0$ in the whole simulation box a circularly polarized plane wave propagating in the z direction and corresponding to the zero order solution [13] given above. The physical parameters are $a_0 = \sqrt{3/2}$ and $n_0/n_c = 0.5$, which corresponds to Fig. 1(b).

The results of the simulation are illustrated in Fig. 4, which shows the time evolution of the scalar potential averaged over two different zones of the wave-vector space corresponding to the first two lobes in Fig. 1(b). The unstable modes grow out of the numerical noise. The development of electrostatic perturbations with growth rates in close agreement with our calculation is a clear signature of the instability. Note also that the naïve 2D extension of Refs. [8–10] predicts a much smaller growth rate for the zone corresponding to our second lobe ($\gamma = 0.06\omega_0$ instead of $\gamma = 0.28\omega_0$).

For $\omega_0 t > 20$, the nonlinear effects of the saturation of the instability cannot be ignored. They lead to an important heating of the electrons, which temperature reaches 100 keV at time $\omega_0 t = 30$. Such a high value of the temperature is not surprising, as the initial jitter energy of an electron in the field of the pump wave is 500 keV.

In conclusion, we present the first calculation of the growth rate of electron parametric instabilities of circularly polarized electromagnetic waves valid for any laser intensity and plasma density. At high density and intensity, the instability extends to large $k_\perp$ with strong growth rates and is associated with the excitation of a wide range of harmonics. Fast filamentation is expected at high density and intensity with transverse size of the order of the laser wavelength. We expect the linearly polarized case to be more complex but to present the same global characteristics. Further developments would imply finite pulse size effects [6,8,10,16], which are out of the scope of the present paper. However, our PIC simulation shows that in the homogeneous case the instability is saturated as soon as $\omega_0 t = 20$, which corresponds to $t = 10$ fs for a 1 μm wavelength. This value is much smaller than typical ultraintense pulses duration, so that we expect that for such pulses the saturation will occur in the body of the pulse.

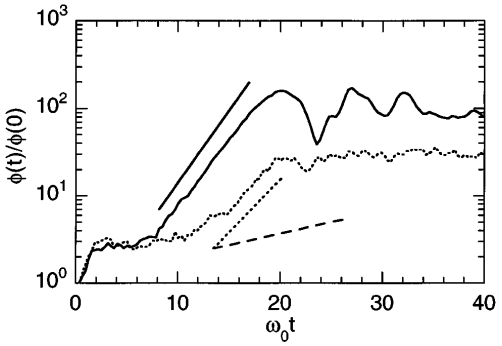

FIG. 4. Time evolution of the scalar potential in two different zones of the wave-vector plane in the PIC simulation for $a_0 = \sqrt{3/2}$ and $n_0/n_c = 0.5$. Solid line: $1.5 \leq k_z c/\omega_0 \leq 2$ and $0 \leq k_\perp c/\omega_0 \leq 0.25$. Dotted line: $2.5 \leq k_z c/\omega_0 \leq 3$ and $1 \leq k_\perp c/\omega_0 \leq 1.3$. The corresponding domains are shown as grey areas on Fig. 1. The slopes of the straight lines correspond to the theoretical value of the growth rate, respectively, $0.38\omega_0$ and $0.28\omega_0$. The dashed line corresponds to the simple 2D extension of Refs. [8–10] for the second domain. Its slope is $0.06\omega_0$.

[1] G. Mourou and D. Umstader, Phys. Fluids B **4**, 2315 (1992).

[2] J. F. Drake *et al.*, Phys. Fluids **17**, 778 (1974); W. L. Kruer, *The Physics of Laser Plasma Interactions* (Addison-Wesley, New York, 1988).

[3] M. Tabak *et al.*, Phys. Plasmas **1**, 1626 (1994).

[4] Special issue on Plasma-Based High-Energy Accelerators, edited by T. Katsouleas, [IEEE Trans. Plasma Sci. **PS-15**, No. 2 (1987), and references therein].

[5] C. J. McKinstrie and R. Bingham, Phys. Fluids B **4**, 2626 (1992).

[6] T. M. Antonsen, Jr. and P. Mora, Phys. Fluids B **5**, 1440 (1993).

[7] N. E. Andreev *et al.*, Phys. Scr. **49**, 101 (1994).

[8] A. S. Sakharov and V. I. Kirsanov, Phys. Rev. E **49**, 3274 (1994).

[9] S. Guérin, G. Laval, P. Mora, J. C. Adam, and A. Héron, Phys. Plasmas **2**, 2807 (1995).

[10] C. D. Decker, W. B. Mori, K. C. Tzeng, and T. Katsouleas, Phys. Plasmas **3**, 2047 (1996).

[11] A. S. Sakharov and V. I. Kirsanov, Plasma Phys. Rep. **21**, 632 (1995).

[12] C. J. Mc Kinstrie and D. F. DuBois, Phys. Fluids **31**, 278 (1988).

[13] A. I. Akhiezer and R. V. Polovin, Sov. Phys. JETP **3**, 696 (1956).

[14] J. Stoer and R. Burlisch, *Introduction to Numerical Analysis* (Springer-Verlag, New York, 1980), pp. 314–404; G. H. Golub and C. F. Van Loan, *Matrix Computations* (John Hopkins University Press, Baltimore, 1989), 2nd ed.

[15] E. Lefebvre and G. Bonnaud, Phys. Rev. Lett. **74**, 2002 (1995); S. Guérin, P. Mora, J. C. Adam, A. Héron, and G. Laval, Phys. Plasmas **3**, 2693 (1996).

[16] K-C. Tzeng, W. B. Mori, and C. D. Decker, Phys. Rev. Lett. **76**, 3332 (1996); E. Esarey *et al.*, Phys. Rev. Lett. **72**, 2887 (1994).